Nanocellulose-based ion-selective membranes for an aqueous organic redox flow battery

Hongli Yang, Penghui Ding, Mikhail Vagin, Viktor Gueskine, Magnus Berggren and Isak Engquist

Cellulose, (2024)
Publisher: Springer
https://doi.org/10.1007/s10570-024-06240-w

Nanocellulose-based ion-selective membranes for an aqueous organic redox flow battery

Hongli Yang,[a,b,1,*] Penghui Ding,[b,1] Mikhail Vagin,[b] Viktor Gueskine,[b,c] Magnus Berggren[b,c] and Isak Engquist [b,c]

[a]*College of Polymer Science and Engineering, Sichuan University, Chengdu 610065, P. R. China.*

[b]*Laboratory of Organic Electronics, Department of Science and Technology, Linköping University, SE-601 74 Norrköping, Sweden*

[c]*Wallenberg Wood Science Centre, Department of Science and Technology, Linköping University, SE-601 74 Norrköping, Sweden*

[1]*These authors contributed equally to this work.*

Corresponding author. E-mail address: yang.hongli@scu.edu.cn

Abstract

The redox flow battery (RFB) has emerged as one of the promising rechargeable energy storage devices. Ion-selective membranes play a pivotal role in RFB regarding their capacity, cycle performance, and cost of production. However, to achieve large-scale commercialization of RFB, it is imperative but remains challenging to develop the next generation of economically efficient and environmentally friendly membranes with outstanding ion transport performance. Here, we report a renewable ion-selective membrane fabricated from wood-derived nanocellulose. The appropriate nanopore size combined with abundant surface charge realized by a chemical cross-linking approach enables membranes with ultralow permeability of redox molecules. As a result, this nanocellulose membrane demonstrates excellent feasibility in an aqueous organic redox flow battery (AORFB) by using 4,5-dihydroxybenzene-1,3-disulfonate as catholyte and alizarin red S as anolyte. More significantly, the nanocellulose membrane indeed outperforms the commercial Nafion 115 membrane including higher capacity and better cycle stability. In addition to the highlighted electrochemical performance of nanocellulose membranes in RFBs, the renewable nanocellulose materials will facilitate AORFB toward sustainable development.

Keywords: nanocellulose; membrane; aqueous organic redox flow battery; energy storage

Introduction

The increasing global demand for clean energy is bringing about a rapid progress in renewable energy conversion technologies such as solar cells, hydroelectric generation, and wind power generation (Østergaard et al. 2020). However, it is difficult for some of these technologies to realize stable supply due to their poor balance between demand and fluctuating generation since they are greatly influenced by environmental factors. Hence, large-scale energy storage devices are required to ensure a stable energy supply by storing intermittent energy resources (Dowling et al. 2020). The redox flow battery (RFB) is one of the promising candidates for grid-scale energy storage device, operating by electrochemically storing the electrical energy in a pair of redox-active species (Dunn et al. 2011; Soloveichik 2015). To commercialize RFBs for large-scale energy storage, crucial parameters are high energy density and long-term operation stability, but we also need to consider the production cost and environmental friendliness (Viswanathan et al. 2014).

A typical RFB contains three main components including porous electrodes, redox molecules dissolved in electrolytes, and membranes (Park et al. 2017). Currently, there are many aqueous soluble organic redox molecules (e.g. quinones) developed to replace the traditional transition metal species (e.g. vanadium) in RFB electrolytes. It is an alternative way to reduce the production cost of RFBs since the abundance of raw materials for organic species enables lower cost of electrolytes than the vanadium system (Winsberg et al. 2017; Wei et al. 2017; Lai et al. 2020). Moreover, aqueous electrolytes offer better safety and sustainability in the practical operation of RFBs compared to the electrolyte with organic solvents (Soloveichik 2015; Park et al. 2017). Another pivotal part of RFBs is the membrane, which not only accounts for the manufacturing cost but also largely determines the final electrochemical performance of RFBs (Noack et al. 2016). The membrane serves as a separator between positive and negative electrolytes to avoid the crossover of active species (ion selectivity), while it also administers the transport of balancing ions to complete the internal circuit (ion conductivity) (Mukhopadhyay et al. 2019; Xiong et al. 2021). Therefore, the fundamental properties of membranes significantly influence the final performance of RFBs, such as capacity retention and cycling stability (Tan et al. 2020). Commercially available ion-exchange membranes, especially perfluorinated sulfonic acid-based Nafion, have often been used in RFBs based on their excellent ion conductivity (Jiang et al. 2016). However, the high crossover of active molecules due to the poor selectivity of Nafion membranes limits the operating life of those RFBs (Lu et al. 2017). Furthermore, the production and waste disposal of expensive and non-

recyclable polyfluorinated chemicals puts dual pressure on the environment and economy (Wang et al. 2017). In addition, researchers have studied membranes based on polyaryletherketone (PAEK) family materials for high performance applications in RFB (Zhang et al. 2023; Zhang et al. 2023; Pinheiro et al. 2023), but the renewability of these materials remains challenging. Therefore, finding low-cost, renewable and environmentally friendly ion-selective membranes with remarkable performance is urgent for the development of RFBs.

Nanocellulose derived from abundant natural resources such as wood is regarded as a type of sustainable, renewable, and low-cost polymer material. There are several inherent structural advantages of nanocellulose used for preparing ion-selective membranes. On one hand, there are abundant hydroxyl groups on the cellulose molecular chains, which provide the ideal platform for various chemical modifications to introduce charged groups (Wågberg et al. 2008; Isogai et al. 2011; Pei et al. 2013). On the other hand, nanofibrils with a high aspect ratio spontaneously form a unique network structure with tunable nanopores, which is beneficial for ion transport and molecule repelling (Wang et al. 2018). Moreover, the excellent mechanical properties including good flexibility and high strength guarantee the stable work of nanocellulose in a variety of battery environments (Li et al. 2021; Lander et al. 2022). However, the nanocellulose materials suffer from swelling in aqueous solutions due to hydrophilic groups, which weaken their structural stability and ion selectivity. Due to the scarcity of research on applying nanocellulose membrane in RFBs, the approach for overcoming the aforementioned bottlenecks is lacking at present.

In this work, we use a method to chemically cross-link the nanocellulose membrane, in which high ion conductivity and selectivity can be simultaneously realized by using 1,2,3,4-butanetetracarboxylic acid (BTCA) as a cross-linker. The cross-linked membrane exhibits good stability even in a strong acidic AORFB system. A comparative performance evaluation was carried out between our membrane and commercial Nafion 115. In an aqueous RFB assembled with 4,5-dihydroxybenzene-1,3-disulfonate (BQDS) as posolyte and alizarin red S (ARS) as negolyte (Fig. S1), the cross-linked nanocellulose membrane was measured to have relatively lower permeability of active molecules, higher capacity, and higher Coulombic efficiency compared to the Nafion membrane.

Experimental section

Materials

Carboxymethylated nanocellulose were provided by the Bioeconomy and Health division at RISE Research Institutes of Sweden. All chemicals including 1, 2, 3, 4-butane tetracarboxylic acid (BTCA), sodium hypophosphite (SHP), glycerol, sulfuric acid (H_2SO_4, 95%–98%), hydrogen peroxide (H_2O_2), sodium hydroxide (NaOH), Alizarin Red S (ARS), and 4,5-dihydroxybenzene-1,3-disulfonate (BQDS) were purchased from Sigma-Aldrich and used as received. Nafion-115 membranes were also purchased from Sigma-Aldrich. The graphite felt (AvCarb G200) was purchased from the Fuel Cell Store (U.S.A.). Experiments were carried out with deionized water.

Preparation of Membranes

The cross-linked nanocellulose membranes were prepared by using the same method as our previously published work (Yang et al. 2022). Before the membrane fabrication, 10 wt% aqueous solutions of BTCA, SHP, and glycerol were prepared. Then the cross-linked membranes with 20 wt% and 33 wt% BTCA dosage were separately prepared. 150 g nanocellulose solution (solid content: 0.5%), 1.875 g BTCA solution, 1.875 g SHP solution, and 0.75 g glycerol solution were mixed together to prepare 20 wt% BTCA cross-linked nanocellulose membrane. Similarly, the mixed solution for 33 wt% BTCA cross-linked nanocellulose membrane was prepared from a mixed solution of 135 g nanocellulose solution, 3.375 g BTCA solution, 3.375 g SHP solution, and 0.675 g glycerol solution. After mixing homogeneously, the solutions were cast in the petri dish with a diameter of 13.5 cm. The bubbles were removed in a vacuum desiccator for two hours. After drying in oven at 60 °C overnight, the obtained membranes were cross-linked through heating at 150 °C for 15 minutes. Finally, the membranes were immersed in deionized water to remove the unreacted species and then dried again. The thickness of obtained nanocellulose membrane was controlled to be around 50 μm. Nafion 115 membrane was pretreated by the following procedures. The membranes were hydrated at 80 °C and then rinsed with water to remove the surface contaminants. Following that, the Nafion membranes were soaked in 3% H_2O_2 for 1 h at 80 °C to remove organic contaminants and then rinsed again with water. The obtained Nafion membranes were soaked in water for 1 h at 80 °C, and thereafter in 1% NaOH for 1 h at 80 °C. The activated Nafion membranes were stored in water and directly used in RFB assembly.

Characterization

Transmission electron microscopy (TEM) image of carboxymethylated nanocellulose was captured using a Tecnai G2 F20 S-TWIN microscope (FEI) with an accelerating voltage of 200 kV. The zeta potential of carboxymethylated nanocellulose particles was measured with a Malvern Zetasizer (Nano ZS) instrument. The Fourier transform infrared spectra of the membrane were performed by employing a Bruker Equinox 55 instrument. The spectra were recorded in the attenuated total reflectance mode with the wavenumber range from 4000 to 400 cm^{-1} and a resolution of 4 cm^{-1}. The mechanical tensile stress-strain curves of the membranes were collected by using a Shimadzu instrument (AGS-X) at room temperature. Water uptake and electrolyte uptake of nanocellulose and Nafion membranes were measured in deionized water and 1 M H_2SO_4 aqueous solution. The membranes were first dried at 100°C overnight and then weighed to obtain their initial mass value in the dry state. These membranes were then soaked in pure water or 1 M H_2SO_4 for 24 hours at room temperature. The wet membranes were weighed after wiping off the excess surface water or H_2SO_4 aqueous solution with cleanroom paper. Each measurement was an average of three different replicated samples. Water/Electrolyte uptake was calculated by the following equation:

$$\text{Water/Electrolyte uptake (\%)} = \frac{W_w - W_d}{W_d} \times 100 \quad (1)$$

where W_w and W_d are the weight of the membrane in the wet and dry state, respectively.

Permeability Measurement

The permeability of redox molecules (BQDS and ARS) across the membranes was measured directly in the same RFB cell studied in this work for 48 hours at the flow rate of 36 mL min^{-1}. 45 mL 0.05 M BQDS or ARS in 1 M H_2SO_4 solution was placed into the donor reservoir and the acceptor reservoir was filled with 45 mL of 1 M H_2SO_4 solution, which were separated by the target membrane. A specific amount of solution was then taken out from the acceptor reservoir for further analysis by UV–visible spectroscopy (Lambda 900, PerkinElmer) every few hours. The anolyte solution would be diluted once their absorbance value deviated from the Beer–Lambert law at high concentration. The absorbance of the characteristic absorption peaks of crossover BQDS (208 nm) and ARS (261 nm) were measured by UV–vis spectroscopy and the permeate concentration of BQDS or ARS was then determined by corresponding calibration curves (Fig. S3-4). The permeability P (cm^2 h^{-1}) could be obtained from a recently reported equation (Li and Lu 2021)

$$ln\left(1-\frac{c_B}{c_A}\right)=-\frac{AP}{LV_B}(t-t_0) \quad (2)$$

where c_A and c_B are the concentrations (M) of BQDS or ARS in the donor and acceptor side, respectively; A and L are the working area (cm^2) and thickness (cm) of the membranes, respectively; V is the volume of the acceptor reservoir (ml); t is the time (h) and t_0 is the time lag (h).

Proton Conductivity

The proton conductivity of membranes was measured by a method of electrochemical impedance spectroscopy (EIS) carried out in a homemade setup. Before the measurements, membranes were soaked in 1 M H_2SO_4 aqueous solution for 24 hours. The membranes were sandwiched by two separated cells equipped with two electrodes made by gold evaporated glass slides. The EIS measurements were executed in 1 M H_2SO_4 aqueous solution with a 10 mV AC amplitude at a frequency range of 100 kHz – 100 mHz by using a potentiostat (BioLogic SP200). The blank cell without a membrane was also measured for calculation. The proton conductivity was calculated according to the following equation:

$$\sigma = \frac{L}{R_m \times A} \quad (3)$$

where L is the membrane thickness; R_m is the resistance calculated by subtracting the resistance of measurement without membrane from the measured resistance with membrane; and A is the membrane working area (28.26 mm^2). The area-specific resistance was calculated by the equation:

$$R = R_m \times A \quad (4)$$

Electrochemical Characterization on Redox Flow Battery

The RFBs were assembled by using a commercial hardware C-flow 5 × 5 (active area: 25 cm^2) purchased from C-Tech Innovation Ltd. (U.K.). The graphite felts used as electrodes and diffusion layers were pretreated under 600 °C (air) for 15 min before the battery assembly. The posolyte was 0.05 M BQDS solution in 1 M H_2SO_4 (30 ml) while the negolyte was 0.05 M ARS solution in 1 M H_2SO_4 (30 ml). The negolyte was first purged with nitrogen to remove oxygen before running and then protected by nitrogen during the whole measurement period. The flow rate controlled by a peristaltic pump (Tygon® LMT-55) was 36 mL min^{-1} that was kept constant for all of the experiments. The charge-discharge procedure of the assembled RFB with different

membranes was performed by using a potentiostat (BioLogic SP200) with a constant current density at room temperature. The refreshing of electrolytes was carried out by pumping the reacted electrolytes back into the tanks after 100 cycles. By following, the assembled cell was clean by flowing deionized water for 12 hours until no color remained in the tank. Then, the water was pumped out, and the fresh electrolytes were pumped back into the tanks again.

Results and discussion

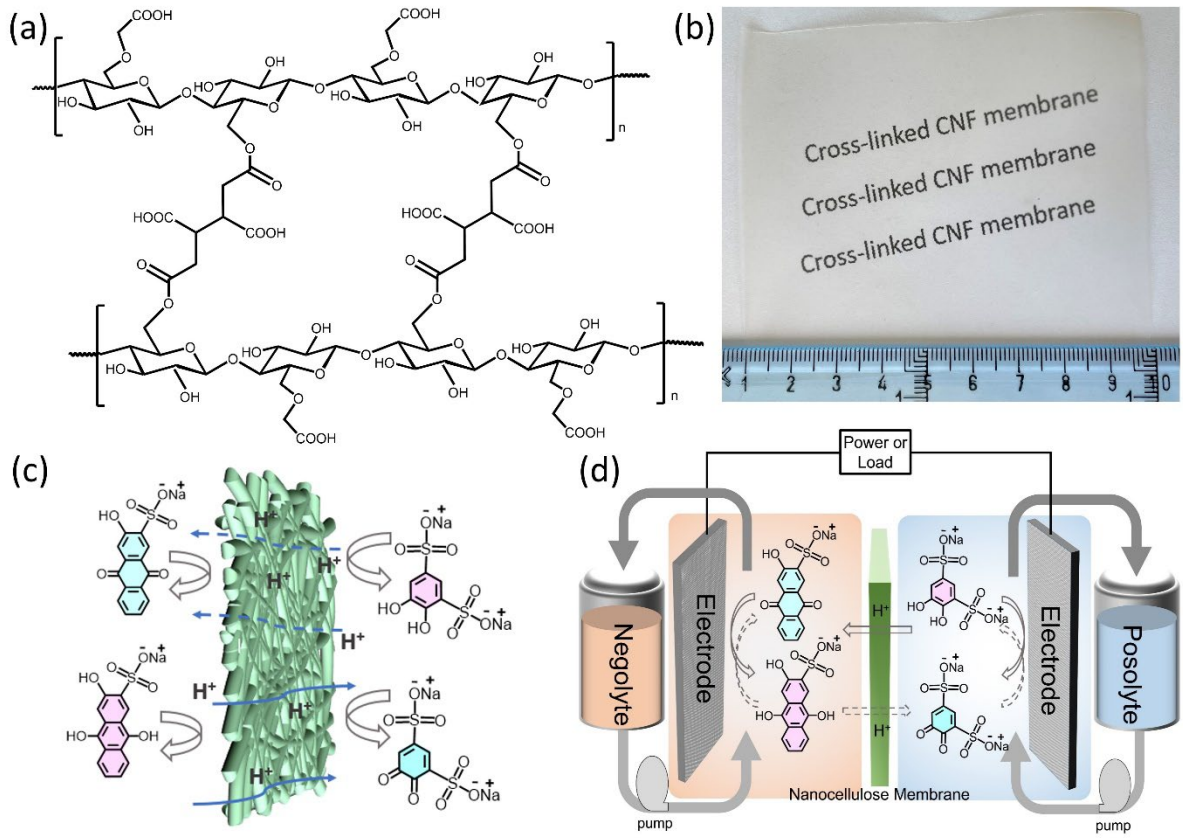

Fig. 1 Structures of nanocellulose membrane and assembled redox flow battery studied in this work. (**a**) Schematic diagram of chemical structure of the cross-linked nanocellulose. (**b**) Photograph of the prepared nanocellulose membrane. (**c**) The working mechanism of the cross-linked nanocellulose membrane in RFB. (**d**) Schematic of a nanocellulose membrane-assembled redox flow battery with BQDS as posolyte and ARS as negolyte.

The nanocellulose membrane was prepared by a one-step esterification reaction between commercially available carboxymethyl nanocellulose, the corresponding TEM image and zeta potential of - 20 mV are shown in Fig. S1a and S1b, respectively, and BTCA, resulting in the cross-linking of cellulose backbones by BTCA molecules (Fig. 1a). This method enables the facile fabrication of large-size freestanding nanocellulose membranes (Fig. 1b). More details

on the membrane preparation procedure can be found in the experimental section and our previous works (Yang et al. 2022). The cross-linking process is expected to improve the electrochemical performance of the obtained membrane in RFB in terms of the following aspects. First, it restricts the swelling of the fibril-entangled network towards better size-exclusion selectivity for redox molecules (Sabzalian et al. 2014). Moreover, it leads to higher proton transport and Donnan exclusion-related ionic selectivity after introducing more charges inside the membrane from the extra unreacted carboxyl groups in BTCA (Fig. 1c). The performance of this nanocellulose membrane was evaluated in an aqueous RFB with an organic couple of ARS and BQDS under an acidic environment (the schematic and photo of RFB system are shown in Fig. 1d and Fig. S2, respectively). Based on our previous work, we selected a BTCA content of 20 wt% to fabricate the membranes, since this concentration previously has been shown to yield cross-linked membranes with optimal ion selectivity, which results from good coordination between the size of nanostructure and charge density in the membranes (Yang et al. 2022). At the same time, the commonly used Nafion 115 membrane was also measured for a comparison study.

Before performing the battery test, several key parameters of both membranes were comparatively studied, such as their crossover performance for redox molecules and proton conductivity, etc. We first measured the permeability of BQDS and ARS through nanocellulose and Nafion 115 membranes since they largely affect the final performance of assembled RFBs. The permeability was determined by single redox-molecule diffusion test under the same flow conditions as in the battery under operation, rather than the static H-cell experiment because crossover performance might change with the operating hydrodynamic system. For the BQDS crossover, the permeability with Nafion 115 membrane was 1.26×10^{-5} cm^2 h^{-1}, but across nanocellulose membrane it decreased by an order of magnitude to 1.65×10^{-6} cm^2 h^{-1} (Fig. 2a, Table S1). Similarly, the nanocellulose membrane displays ca. 8.3 times less ARS crossover than Nafion 115 membrane (Fig. 2b, Table S1). These results reveal that the nanocellulose membranes have a better capability to limit crossover compared with the commercial Nafion 115 membrane.

The through-plane proton conductivity of membranes was evaluated by electrochemical impedance spectroscopy in 1 M H_2SO_4 aqueous electrolyte (the obtained *Nyquist* plots are shown in Fig. 2c). The calculated proton conductivity (detailed calculation method is provided in the experimental section) of Nafion 115 and nanocellulose membrane is 1.94×10^{-2} S cm^{-1} and 2.13×10^{-3} S cm^{-1}, respectively. The lower proton conductivity of nanocellulose membrane compared to that of Nafion can be attributed to the weaker proton conducting ability of carboxyl

groups and the difference in their intrinsic structures that were also reported in other literature (Bayer et al. 2016; Guccini et al. 2019). Even so, it is worth noting that the area-specific resistance of the nanocellulose membrane (3.29 Ω cm^2) is comparable to that of the Nafion membrane (0.73 Ω cm^2) benefiting from the lower thickness of the nanocellulose membrane.

The mechanical performance of the membrane is also a significant concern for the long-term operating stability of RFB. A tensile experiment was performed to evaluate the mechanical properties of the nanocellulose membrane, whose resulting stress-strain curve was compared with Nafion 115 membrane as shown in Fig. 2d. Young's modulus of nanocellulose membrane reaches up to 1.8 GPa, an order of magnitude higher than that of Nafion 115 (0.1 GPa), demonstrating superior resistance to deformation of the nanocellulose membrane. Although with smaller elongation at a break (~7%), the tensile strength at the break of nanocellulose membrane was measured to be around 90 MPa, much higher than that of Nafion 115 membrane (25 MPa). This indicates that the mechanical strength of nanocellulose membrane is high, and appropriate for meeting the practical requirement of RFB.

To investigate the swelling behavior of membranes in aqueous environment, water uptake as well as electrolyte uptake in H_2SO_4 solution of nanocellulose and Nafion 115 membranes were measured (Fig. S5). Compared to that of Nafion 115 membrane, the nanocellulose membrane shows a higher value of water uptake resulting from its intrinsic hydrophilicity. However, the electrolyte uptake of the nanocellulose membrane dramatically decreases once increasing the acid concentration. For the electrolyte uptake in 1 M H_2SO_4 aqueous solution, the value of nanocellulose membrane (21.9 ± 1.7%) is very close to that of Nafion 115 membrane (19.6 ± 2.2%). In this case, the swelling of the membrane is mainly dominated by the electrostatic repulsion between charged groups inside the membrane. The carboxyl groups on cellulose chains and BTCA are weak acids with higher pKa (pKa of BTCA at 25°C, pK1: 3.43; pK2: 4.58; pK3: 5.85; pK4: 7.16). It indicates a negligible degree of dissociation of carboxyl groups in 1 M H_2SO_4 solution, leading to weak electrostatic repulsions inside the nanocellulose membrane. Therefore, the nanocellulose membrane shows a low electrolyte uptake at a higher acid concentration compared with the pure water uptake, which is beneficial for the operation of RFB studied in this work since low electrolyte uptake can limit the crossover of redox active species.

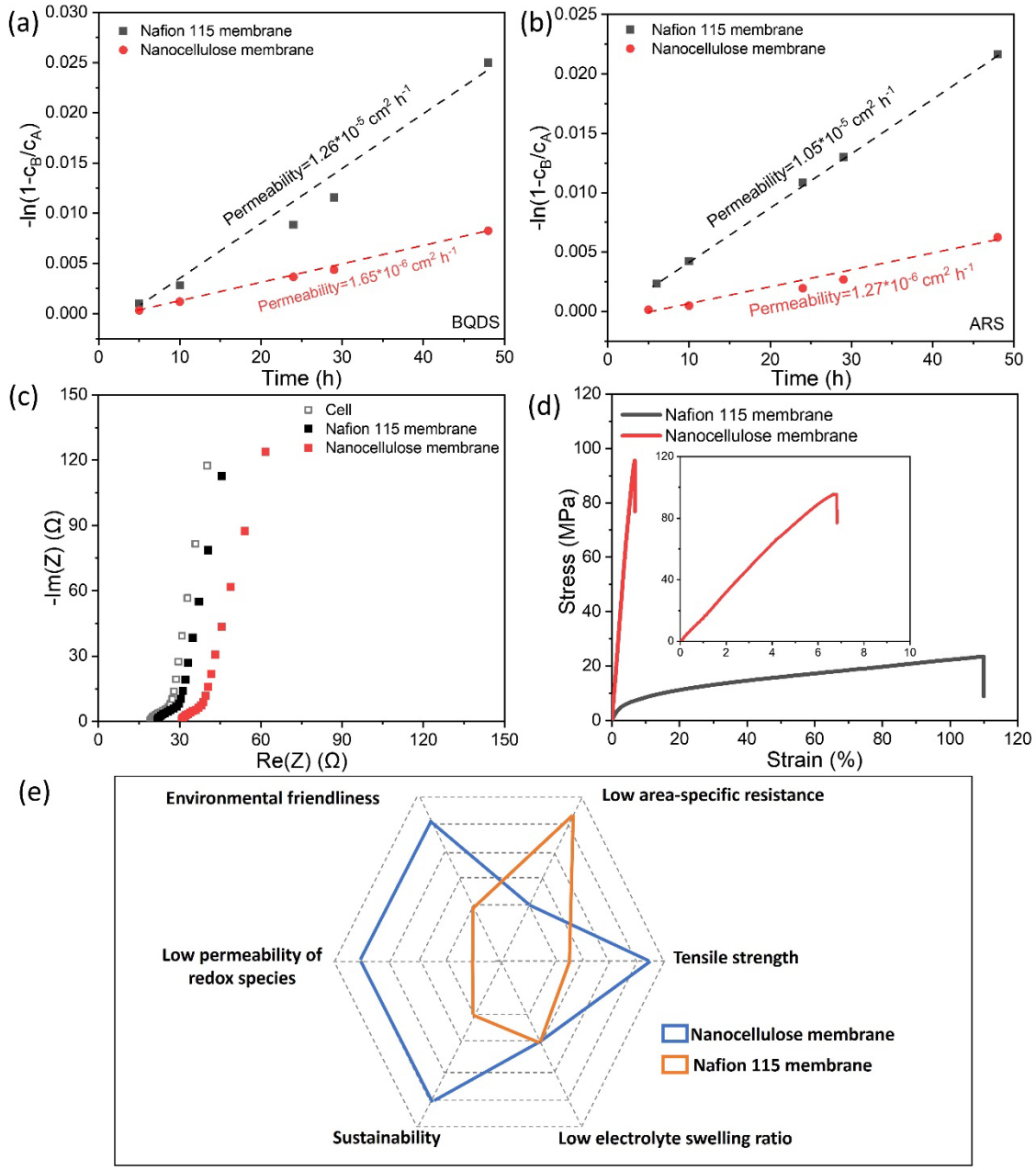

Fig. 2 Comparison study of various parameters between nanocellulose membrane with thickness of 50 µm and Nafion 115 membrane with thickness of 127 µm. Permeation kinetic curves (*-ln (1-c_B/c_A)* versus permeation time) for determining the permeability of (**a**) BQDS and (**b**) ARS through nanocellulose and Nafion 115 membranes, respectively. The slope values used to determine the permeability values under flow in (**a**) and (**b**) are obtained by linear fitting. (**c**) *Nyquist* plots of the blank cell and cell with nanocellulose and Nafion 115 membranes in 1 M H_2SO_4. (**d**) Mechanical tensile curves of nanocellulose and Nafion 115 membranes (inset: zoom-in stress-strain curve of the nanocellulose membrane). (**e**) Qualitative ranking of key performance indicators for nanocellulose and Nafion 115 membranes, whose detailed parameters can be found in Table S2.

Considering all of the aforementioned parameters, a comprehensive comparison between the nanocellulose membrane and Nafion 115 membrane can be summarized as shown in Fig. 2e and Table S2. The nanocellulose membrane exhibits prominent performance advantages compared to Nafion 115 membrane, including lower redox molecule crossover, higher mechanical strength, and better sustainability merits. Meanwhile, the nanocellulose membrane demonstrates comparable area-specific resistance and a similar swelling ratio in acidic electrolyte compared to Nafion. Therefore, the nanocellulose membrane is expected to be a competitive membrane candidate for substituting the expensive Nafion membrane in RFB.

The electrochemical cycling performance of RFBs with nanocellulose and Nafion 115 membranes was evaluated by performing the charge-discharge cycling test at a current density of 4 mA cm^{-2}, from which the discharge capacity and Coulombic efficiency can be derived. Fig. 3a and 3b show typical charge-discharge voltage profiles at the 1^{st}, 50^{th}, and 100^{th} cycles of RFB using nanocellulose membrane and Nafion 115 membrane, respectively. The calculated discharge capacity and Coulombic efficiency are summarized in Fig. 3c and Fig. 3d, respectively. The RFB with nanocellulose membrane shows both a slightly higher discharge capacity and a slightly higher Coulombic efficiency compared to the one with Nafion 115 membrane, during the entire 100 cycles. This can be attributed to the lower ARS and BQDS permeability of the nanocellulose membrane compared to that of the Nafion membrane. The advantage relies on having an appropriate nanopore size in the nanocellulose membrane for better redox-molecule repelling, which can be further verified by using a nanocellulose membrane with larger nanopore size (33 wt% BTCA) as a contrasting sample that exhibits lower cycling capacity and Coulombic efficiency (Fig. S6). According to our previous work, the membrane with 33 wt% BTCA has a larger nanopore size and reduced ion selectivity compared to those of the 20 wt% BTCA membrane in the wet state (Yang et al. 2022).

Generally, in addition to the crossover of redox molecules through membranes, there is another reason for fading of the electrochemical cycling capacity of RFBs: decomposition or adverse chemical reactions of the redox couples, some researchers have reported the severe degradation of BQDS during cycling due to the Michael reactions (Yang et al. 2016; Lander et al. 2024). As a result, there is a 47% capacity reduction in RFB after 100 charge-discharge cycles, as shown in Fig. 3c. This problem can be usually handled by refreshing the electrolyte, and the detailed process for refreshing electrolytes is shown in Experimental section. We therefore performed an experiment where the electrolytes were refreshed every 100 cycles. The discharge capacity, Coulombic efficiency (CE) and voltage efficiency (VE) of the RFBs with nanocellulose and Nafion 115 membranes were measured, with results shown in Fig. 3c and

Fig. 3d, respectively. The graphs clearly show that the discharge capacity can be close to fully recovered, since they are almost identical (~25 mAh) at the 1st cycle and at cycles 101 and 201 (Fig. 3c). It means the battery performance can be nearly recovered after refreshing the electrolytes, indicating that the capacity reduction after 100 cycles mainly results from the decomposition of redox molecules in electrolyte. During the first and second 100 cycles, VE of the RFBs with Nafion 115 membrane was higher than that with nanocellulose membrane due to higher resistance of nanocellulose membrane. In addition, CE and VE can be recovered after twice refreshing electrolytes in the RFB assembled with nanocellulose membrane. However, after the second refresh of electrolyte, there are varying degrees of decay for discharge capacity, CE and VE in the RFB using Nafion 115 membrane, which might be caused by the Nafion membrane fouling as shown in Fig. 4a. By comparison, the cycle performance of the RFB with nanocellulose membrane is almost unchanged after twice electrolyte refreshing, exhibiting better stability.

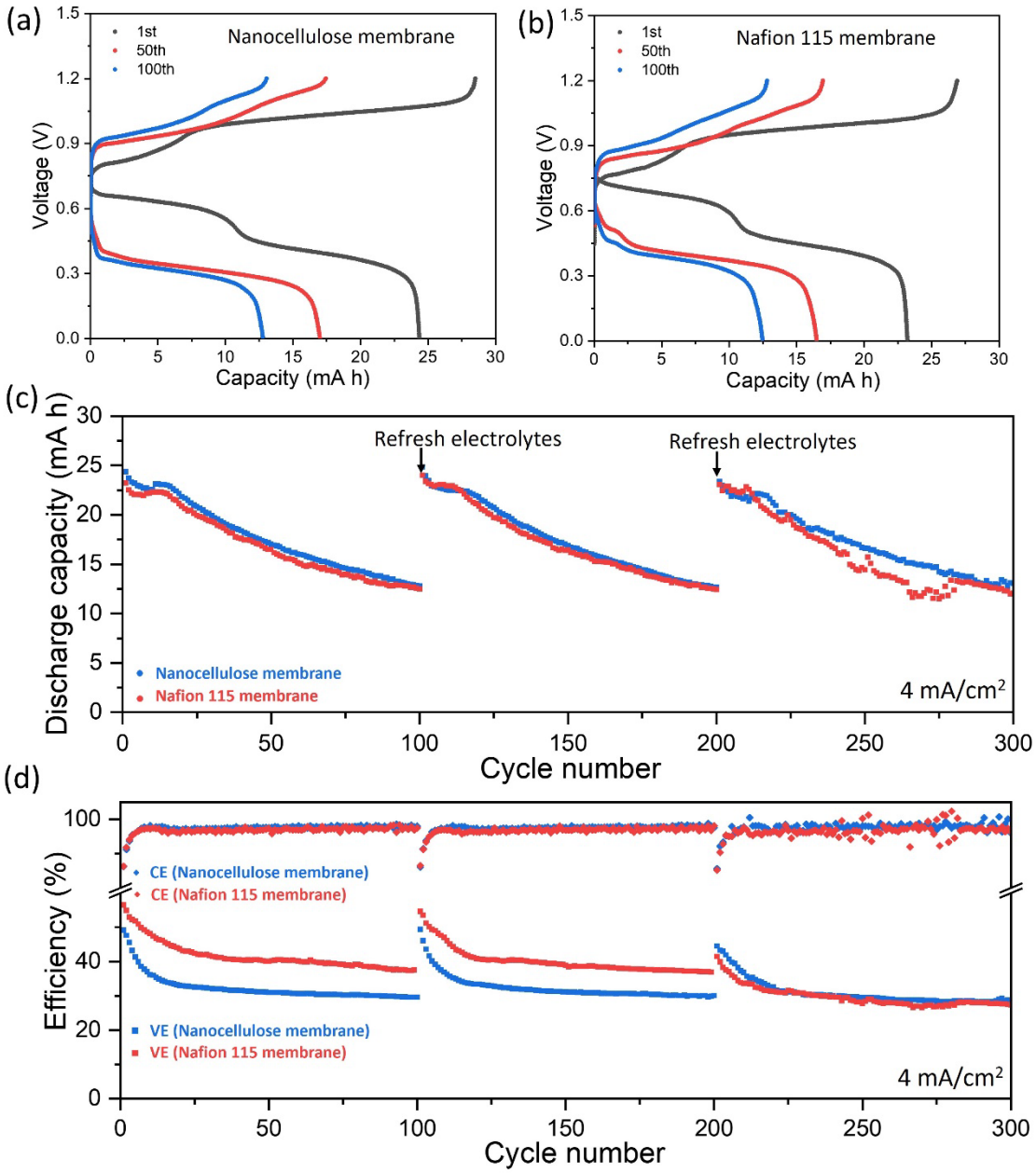

Fig. 3 Electrochemical cycling performance of RFB by using nanocellulose and Nafion 115 membranes, respectively. Charge-discharge voltage profiles of RFB at the 1st, 50th, and 100th cycle by using (**a**) nanocellulose and **(b**) Nafion 115 membrane. Cycling stability regarding (**c**) discharge capacity and (**d**) Coulombic efficiency (CE) and voltage efficiency (VE) of RFB by using nanocellulose and Nafion 115 membranes under the initial 100 cycles and two more 100 cycles after refreshed electrolytes. All results in Fig. 3 were collected at a current density of 4 mA cm^{-2}.

The current rate performance of RFBs with nanocellulose membrane and Nafion 115 membrane was also investigated, at different current densities (Fig. 4). The discharge capacity of RFB with nanocellulose membrane decreases from 25 mAh to 7 mAh when increasing the current density from 4 mA cm^{-2} to 20 mA cm^{-2}, demonstrating similar and slightly better rate performance than that of RFB with Nafion. The reduction of capacity for both membranes with the increase of current density is possibly attributed to limited mass transport and increased overpotential at higher current densities (Mukhopadhyay et al. 2021). Significantly, the RFB with nanocellulose membrane consistently shows higher discharge capacity and CE than that of RFB with Nafion 115 membrane at different current densities, indicating better ion selectivity combined with less crossover of active molecules and lower capacity loss. However, the VE and energy efficiency (EE) were slightly lower in RFB with nanocellulose membrane. This can be attributed to the relatively lower proton conductivity and higher resistance of the nanocellulose membrane. Considering the tradeoff between the crossover performance and ionic resistance of membranes, the overall performance under different current densities of the RFB with nanocellulose membrane is comparable with that of RFB with Nafion 115 membrane in this acidic ARS and BQDS system (Fig. 4).

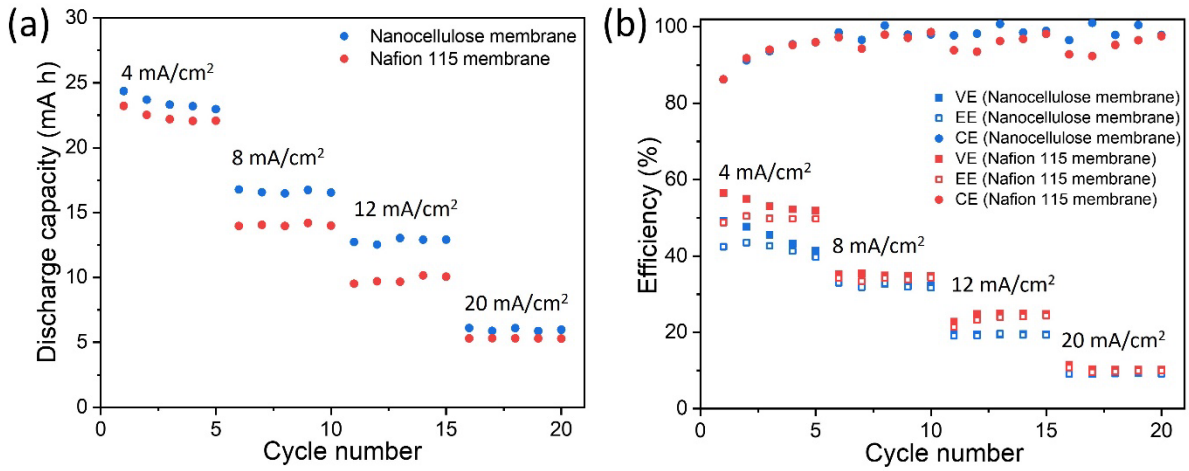

Fig. 4 The current rate performance of RFBs with nanocellulose membrane and Nafion 115 membrane. (a) The discharge capacity of RFBs versus cycle number at different current densities. (b) Coulombic efficiency, voltage efficiency, and energy efficiency of RFBs versus cycle number at different current densities.

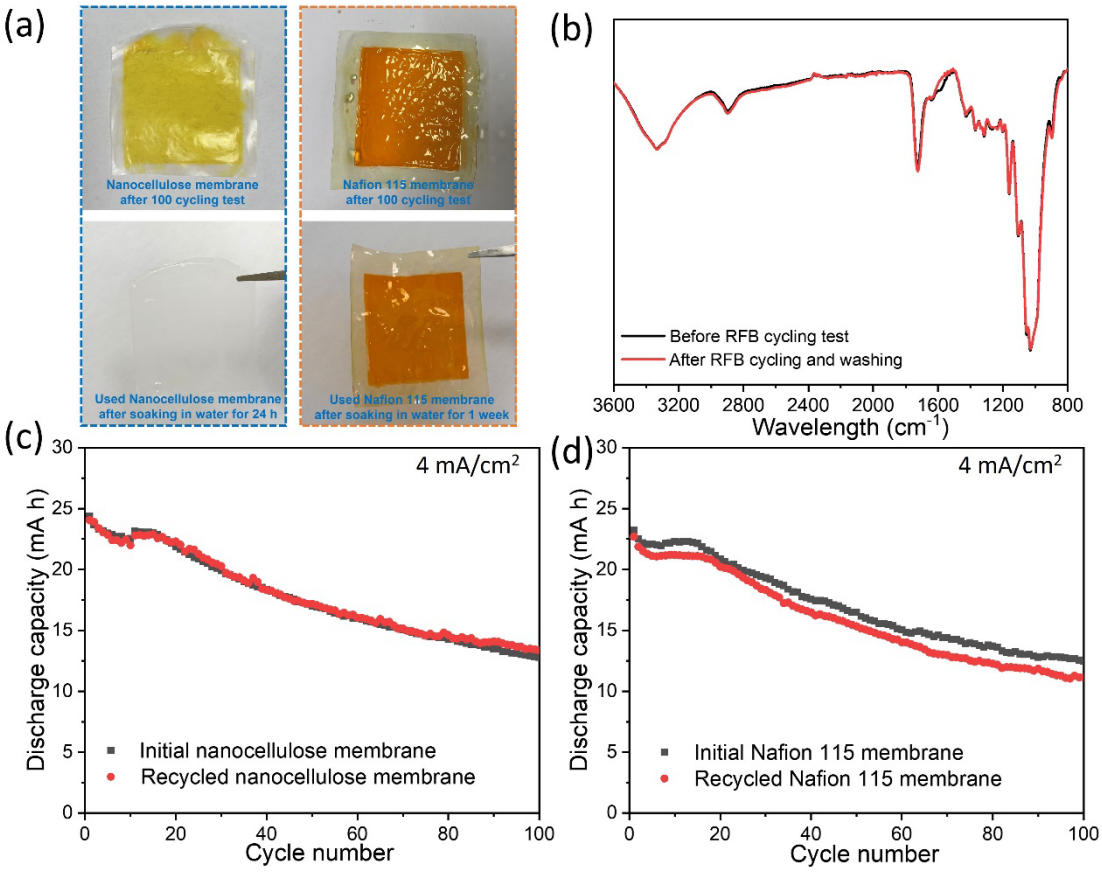

Fig. 5 The comparison study on the recyclability of nanocellulose and Nafion 115 membranes. (**a**) Digital images of recycled nanocellulose membrane (left) and Nafion 115 membrane (right). (**b**) ATR-FTIR spectra of the nanocellulose membrane before the RFB cycling test and after the RFB cycling test and washing. Cycling stability regarding discharge capacity by using fresh and recycled (**c**) nanocellulose membrane and (**d**) Nafion 115 membrane under 100 cycles with current density of 4 mA cm^{-2}.

The recyclability of the membrane after the operation of the RFB is likewise an important aspect since it directly influences sustainability and economic efficiency. Both nanocellulose and Nafion 115 membranes were colored after 100 test cycles due to the absorption of redox molecules, as shown in Fig. 5a. However, the Nafion 115 membrane has a deeper color compared with the nanocellulose membranes. Surprisingly, we found that the coloring of the nanocellulose membrane could be totally removed by immersing it in water for 6 hours. By contrast, the Nafion membrane was still colored even after immersing in water for one week (Fig. 4a), indicating the severe membrane fouling process of Nafion membrane. The membrane fouling is the process that redox molecules attach to the membrane by absorption, causing the block of ion-selective sites in the membrane, which further impairs the RFB performance

(Vijayakumar et al. 2011; Gao et al. 2022). To confirm the stability of the nanocellulose membrane, Fourier transform infrared spectroscopy was employed before and after the RFB cycling test and subsequent washing in water. Two almost identical spectra of the nanocellulose membrane before and after cycling+washing can be clearly observed in Fig. 5b and Fig. S7, revealing the excellent chemical stability of nanocellulose membrane in this RFB system. The only perceptible changes between the two spectra are the slightly increased strength of the peak at around 1725 cm^{-1} (corresponding to the C=O stretching) and the disappearance of the peak at around 1580 cm^{-1} (also related to the C=O stretching vibration). These changes can be attributed to the complete protonation of carboxylate groups in the nanocellulose membrane after cycling in a strong acidic environment of RFB. As a final test, the recycled nanocellulose membrane after cleaning by water was assembled again into the RFB for further electrochemical cycling. As shown in Fig. 5c, the cycling performance of the RFB with recycled nanocellulose membrane is almost identical with the original nanocellulose membrane. In contrast, the RFB with recycled Nafion 115 membrane (immersed in water for one week) shows obvious performance degradation (Fig. 5d), deriving from Nafion membrane fouling process. There is not only a decrease of the overall discharge capacity during the cycling, but also a reduction of capacity retention after 100 cycles. The results indicate that nanocellulose membrane shows outstanding recyclability during the RFB operation.

Conclusions

In summary, we have demonstrated a high-performance nanocellulose membrane for aqueous RFB, with potential for lower cost than relevant commercial membranes. The chemical cross-linking enables nanocellulose membranes with excellent structural stability in aqueous solution, as well as a combination of high ionic conductivity and low crossover of redox molecules due to the coupling effect between abundant surface charge and nano-porous structure. By systematic comparison with commercial Nafion 115 membrane in a proof-of-concept RFB based on BQDS and ARS electrolytes, the nanocellulose membrane has been verified to have better electrochemical performance than the Nafion membrane. Most significantly, the nanocellulose membrane can be completely regenerated after use in an aqueous RFB, without any performance decay. This work provides a sustainable and economy-efficient way to process natural materials into high value-added membranes applicable in RFB.

Acknowledgments

This work was financially supported by VINNOVA (Digital Cellulose Centre) and the Knut and Alice Wallenberg Foundation (Wallenberg Wood Science Center). The authors also acknowledge RISE Bioeconomy and Health for the supply of carboxymethylated nanocellulose.

Declarations

Ethical approval Not applicable.

Competing interests The authors declare no competing interests.

Funding

The Funding was provided by VINNOVA (Digital Cellulose Centre) and the Knut and Alice Wallenberg Foundation (Wallenberg Wood Science Center).

References

Bayer T, Cunning BV, Selyanchyn R, et al (2016) High temperature proton conduction in nanocellulose membranes: paper fuel cells. Chem Mater 28:4805–4814. https://doi.org/10.1021/acs.chemmater.6b01990

Dowling JA, Rinaldi KZ, Ruggles TH, et al (2020) Role of long-duration energy storage in variable renewable electricity systems. Joule 4:1907–1928. https://doi.org/10.1016/j.joule.2020.07.007

Dunn B, Kamath H, Tarascon J-M (2011) Electrical energy storage for the grid: a battery of choices. Science 334:928–935. https://doi.org/10.1126/science.1212741

Gao M, Salla M, Zhang F, et al (2022) Membrane fouling in aqueous redox flow batteries. J Power Sources 527:231180. https://doi.org/10.1016/j.jpowsour.2022.231180

Guccini V, Carlson A, Yu S, et al (2019) Highly proton conductive membranes based on carboxylated cellulose nanofibres and their performance in proton exchange membrane fuel cells. J Mater Chem A 7:25032–25039. https://doi.org/10.1039/C9TA04898G

Isogai A, Saito T, Fukuzumi H (2011) TEMPO-oxidized cellulose nanofibers. Nanoscale 3:71–85. https://doi.org/10.1039/C0NR00583E

Jiang B, Wu L, Yu L, et al (2016) A comparative study of Nafion series membranes for vanadium redox flow batteries. J Membr Sci 510:18–26. https://doi.org/10.1016/j.memsci.2016.03.007

Lai YY, Li X, Liu K, et al (2020) Stable low-cost organic dye anolyte for aqueous organic redox flow battery. ACS Appl Energy Mater 3:2290–2295. https://doi.org/10.1021/acsaem.9b01735

Lander S, Erlandsson J, Vagin M, et al (2022) Sulfonated cellulose membranes: physicochemical properties and ionic transport versus degree of sulfonation. Adv Sustain Syst 6: 2200275. https://doi.org/10.1002/adsu.202200275

Lander S, Pang J, Erlandsson J, et al (2024) Controlling the rate of posolyte degradation in all-quinone aqueous organic redox flow batteries by sulfonated nanocellulose based membranes: The role of crossover and Michael addition. J Energy Storage 83:110338. https://doi.org/10.1016/j.est.2023.110338

Li T, Chen C, Brozena AH, et al (2021) Developing fibrillated cellulose as a sustainable technological material. Nature 590:47–56. https://doi.org/10.1038/s41586-020-03167-7

Li Z, Lu Y-C (2021) Polysulfide-based redox flow batteries with long life and low levelized cost enabled by charge-reinforced ion-selective membranes. Nat Energy 6:517–528. https://doi.org/10.1038/s41560-021-00804-x

Lu W, Yuan Z, Zhao Y, et al (2017) Porous membranes in secondary battery technologies. Chem Soc Rev 46:2199–2236. https://doi.org/10.1039/C6CS00823B

Mukhopadhyay A, Cheng Z, Natan A, et al (2019) Stable and highly ion-selective membrane made from cellulose nanocrystals for aqueous redox flow batteries. Nano Lett 19:8979–8989. https://doi.org/10.1021/acs.nanolett.9b03964

Mukhopadhyay A, Yang Y, Cheng Z, et al (2021) Proton-conductive membranes with percolated transport paths for aqueous redox flow batteries. Mater Today Nano 13:100100. https://doi.org/10.1016/j.mtnano.2020.100100

Noack J, Wietschel L, Roznyatovskaya N, et al (2016) Techno-economic modeling and analysis of redox flow battery systems. Energies 9:627. https://doi.org/10.3390/en9080627

Østergaard PA, Duic N, Noorollahi Y, et al (2020) Sustainable development using renewable energy technology. Renew Energ 146:2430–2437. https://doi.org/10.1016/j.renene.2019.08.094

Park M, Ryu J, Wang W, Cho J (2017) Material design and engineering of next-generation flow-battery technologies. Nat Rev Mater 2:16080. https://doi.org/10.1038/natrevmats.2016.80

Pei A, Butchosa N, Berglund LA, Zhou Q (2013) Surface quaternized cellulose nanofibrils with high water absorbency and adsorption capacity for anionic dyes. Soft Matter 9:2047. https://doi.org/10.1039/c2sm27344f

Pinheiro D, Sousa J. F, Pineiro M, et al (2023) Non-pre-treated sulfonated poly (ether ether ketone) membrane as an efficient alternative for Nafion in acidic aqueous organic redox flow batteries. J Energy Storage 57: 106201. https://doi.org/10.1016/j.est.2022.106201

Sabzalian Z, Alam MN, Van De Ven TGM (2014) Hydrophobization and characterization of internally crosslink-reinforced cellulose fibers. Cellulose 21: 1381-1393. https://doi.org/10.1007/s10570-014-0178-6

Soloveichik GL (2015) Flow batteries: current status and trends. Chem Rev 115:11533–11558. https://doi.org/10.1021/cr500720t

Tan R, Wang A, Malpass-Evans R, et al (2020) Hydrophilic microporous membranes for selective ion separation and flow-battery energy storage. Nat Mater 19:195–202. https://doi.org/10.1038/s41563-019-0536-8

Vijayakumar M, Bhuvaneswari MS, Nachimuthu P, et al (2011) Spectroscopic investigations of the fouling process on Nafion membranes in vanadium redox flow batteries. J Membr Sci 366:325–334. https://doi.org/10.1016/j.memsci.2010.10.018

Viswanathan V, Crawford A, Stephenson D, et al (2014) Cost and performance model for redox flow batteries. J Power Sources 247:1040–1051. https://doi.org/10.1016/j.jpowsour.2012.12.023

Wågberg L, Decher G, Norgren M, et al (2008) The build-up of polyelectrolyte multilayers of microfibrillated cellulose and cationic polyelectrolytes. Langmuir 24:784–795. https://doi.org/10.1021/la702481v

Wang C, Wang S, Chen G, et al (2018) Flexible, bio-compatible nanofluidic ion conductor. Chem Mater 30:7707–7713. https://doi.org/10.1021/acs.chemmater.8b03006

Wang Z, DeWitt JC, Higgins CP, Cousins IT (2017) A never-ending story of per- and polyfluoroalkyl substances (PFASs)? Environ Sci Technol 51:2508–2518. https://doi.org/10.1021/acs.est.6b04806

Wei X, Pan W, Duan W, et al (2017) Materials and systems for organic redox flow batteries: status and challenges. ACS Energy Lett 2:2187–2204. https://doi.org/10.1021/acsenergylett.7b00650

Winsberg J, Hagemann T, Janoschka T, et al (2017) Redox-flow batteries: from metals to organic redox - active materials. Angew Chem Int Ed 56:686–711. https://doi.org/10.1002/anie.201604925

Xiong P, Zhang L, Chen Y, et al (2021) A chemistry and microstructure perspective on ion-conducting membranes for redox flow batteries. Angew Chem Int Ed 60:24770–24798. https://doi.org/10.1002/anie.202105619

Yang B, Hoober-Burkhardt L, Krishnamoorthy S, et al (2016) High-performance aqueous organic flow battery with quinone-based redox couples at both electrodes. J Electrochem Soc 163:A1442–A1449. https://doi.org/10.1149/2.1371607jes

Yang H, Edberg J, Gueskine V, et al (2022) The effect of crosslinking on ion transport in nanocellulose-based membranes. Carbohydr Polym 278:118938. https://doi.org/10.1016/j.carbpol.2021.118938

Zhang B, Yang Z, Liu Q, et al (2023) Swelling-induced cross-linked pyridine-containing membranes with high stability and conductivity for vanadium redox flow batteries. ACS Sustain Chem Eng 11: 11601-11612. https://doi.org/10.1021/acssuschemeng.3c02436

Zhang B, Zhang X, Liu Q, et al (2023) Robust selective swelling-induced pyridine-containing membranes with advanced conductivity for vanadium redox flow batteries. J Power Sources 580: 233360. https://doi.org/10.1016/j.jpowsour.2023.233360

Supporting Information

Nanocellulose-based ion-selective membranes for an aqueous organic redox flow battery

Hongli Yang,[a,b,1,*] Penghui Ding,[b,1] Mikhail Vagin,[b] Viktor Gueskine,[b,c] Magnus Berggren[b,c] and Isak Engquist [b,c]

[a]*College of Polymer Science and Engineering, Sichuan University, Chengdu 610065, P. R. China.*

[b]*Laboratory of Organic Electronics, Department of Science and Technology, Linköping University, SE-601 74 Norrköping, Sweden*

[c]*Wallenberg Wood Science Centre, Department of Science and Technology, Linköping University, SE-601 74 Norrköping, Sweden*

[1]*These authors contributed equally to this work.*

Corresponding author. E-mail address: yang.hongli@scu.edu.cn

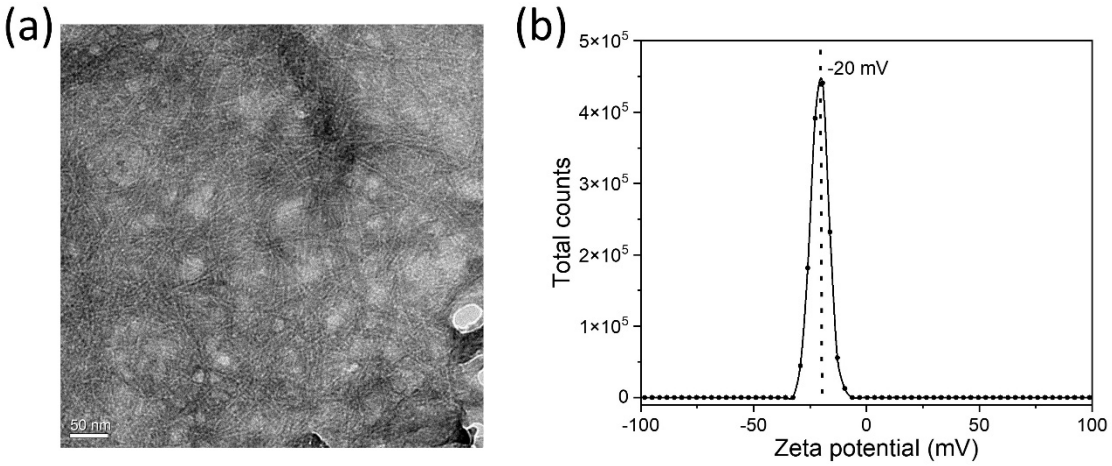

Fig. S1 (a) TEM image and (b) zeta potential of carboxymethylated nanocellulose.

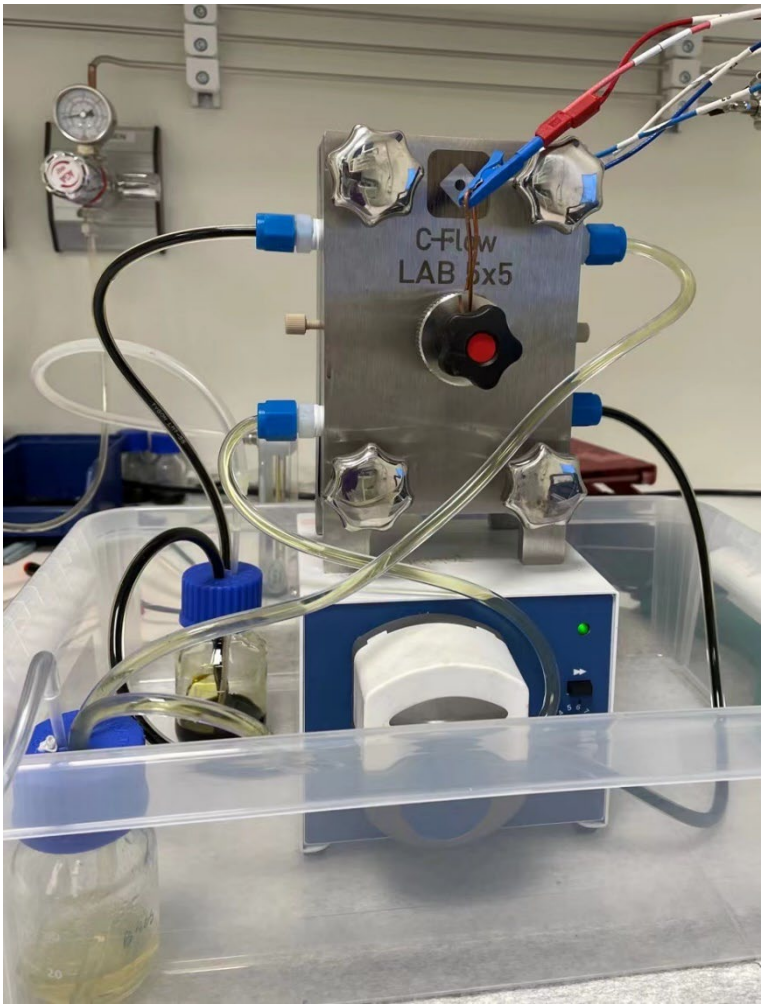

Fig. S2 Digital image of the flow battery system assembled with tiron as posolyte and alizarin red S as negolyte.

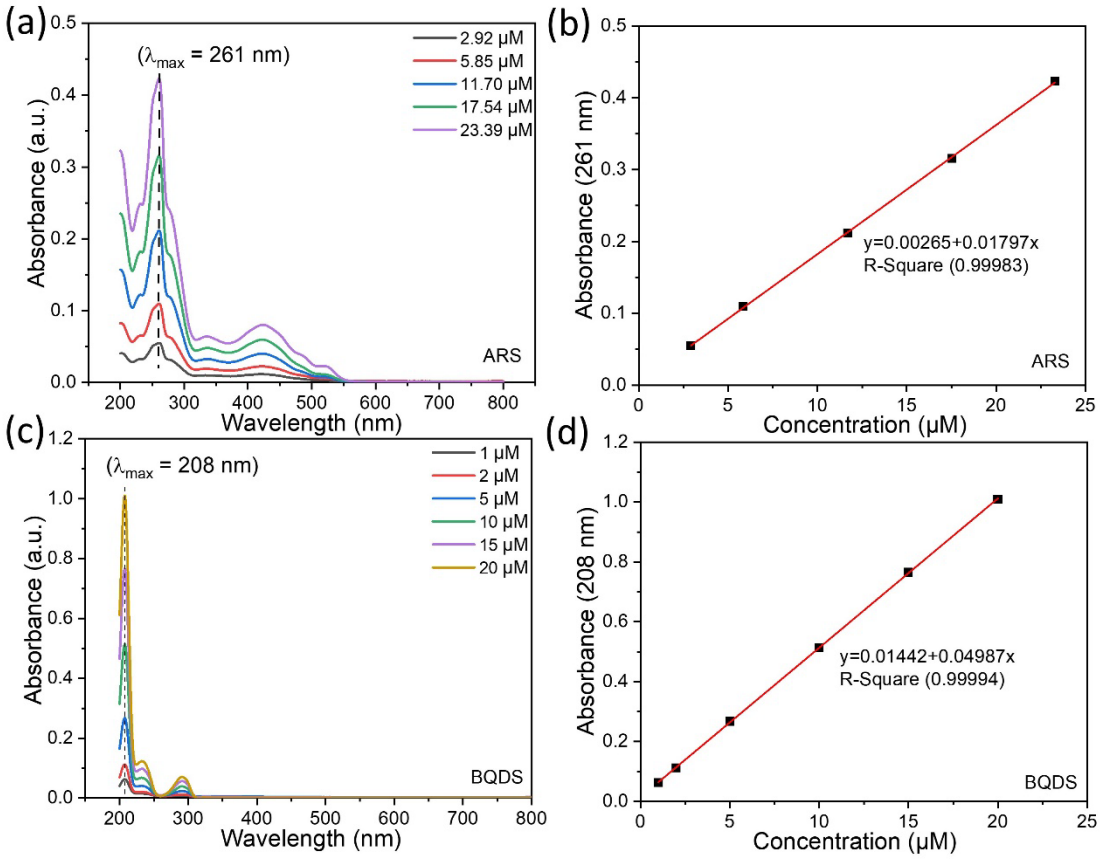

Fig. S3 (a) UV–visible spectra of ARS solution under multiple concentrations between 2.92 μM to 23.39 μM in 1 M H_2SO_4. (b) Beer's law plot for ARS is based on the peak absorbance at 261 nm. (c) UV–visible spectra of BQDS solution under multiple concentrations between 1 μM to 20 μM in 1 M H_2SO_4. (d) Beer's law plot for BQDS is based on the peak absorbance at 208 nm.

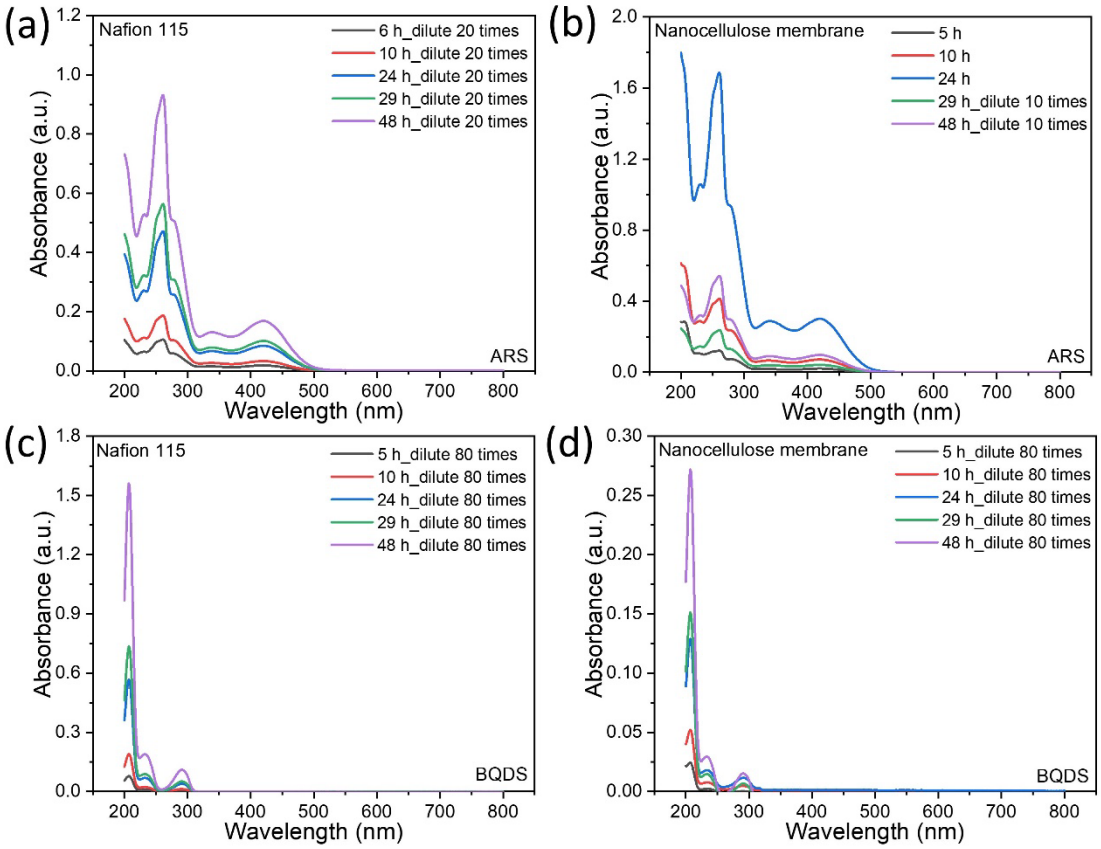

Fig. S4 UV–visible spectra of acceptor solutions with permeated ARS in 1 M H_2SO_4 (the spectra were tested after the acceptor solutions were diluted different times) tested through (a) Nafion 115 membrane and (b) nanocellulose membrane. UV–visible spectra of acceptor solutions with permeated BQDS in 1 M H_2SO_4 (the spectra were tested after acceptor solutions were diluted 80 times) tested through (c) Nafion 115 membrane and (d) nanocellulose membrane.

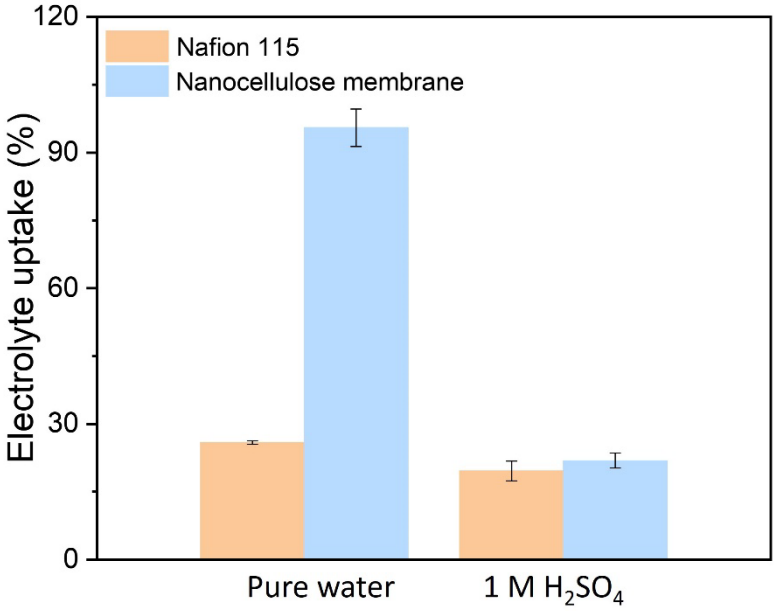

Fig. S5 Water and electrolyte uptake of nanocellulose and Nafion 115 membranes.

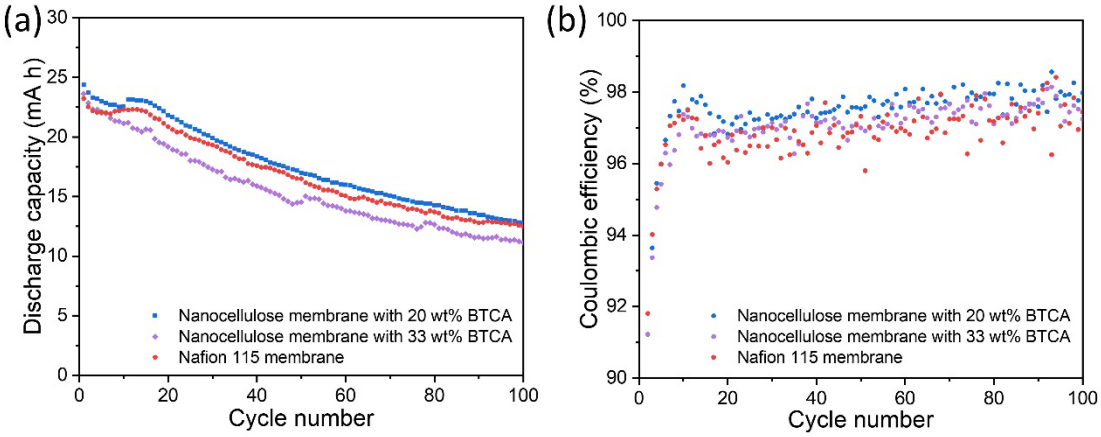

Fig. S6 Cycling performance of the RFBs regarding (a) discharge capacity, and (b) Coulombic efficiency by using nanocellulose (with different cross-linker mass ratios) and Nafion 115 membranes at a current density of 4 mA cm^{-2}.

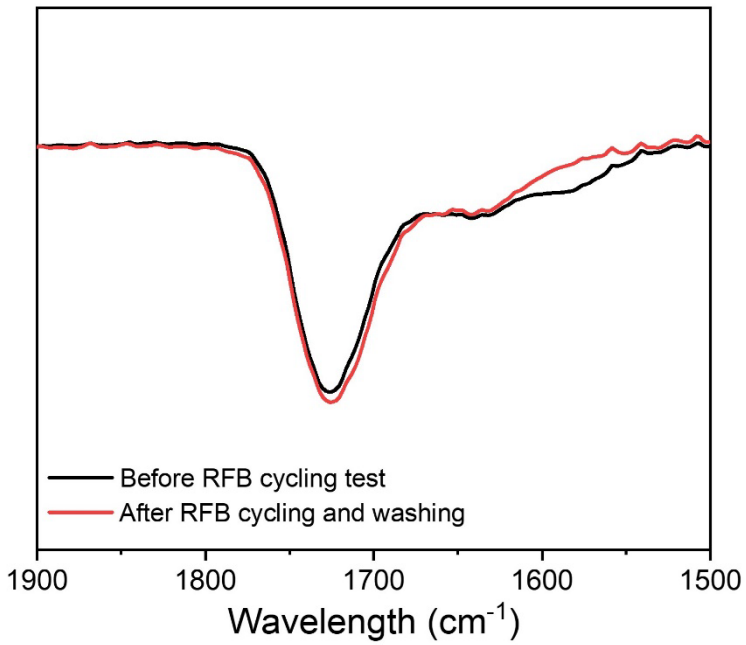

Fig. S7 ATR-FTIR spectra of the nanocellulose membrane before the RFB cycling test and after the RFB cycling and washing.

Table S1 Parameters of $-ln\ (1-c_B/c_A)$ vs. permeation time plots in Figure 2a and 2b.

Membrane	**Thickness** (μm)	**Redox species**	**Slope** (h^{-1})	**Permeability** ($cm^2\ h^{-1}$)
Nanocellulose	50	BQDS	$1.83*10^{-4}$	$1.65*10^{-6}$
		ARS	$1.41*10^{-4}$	$1.27*10^{-6}$
Nafion 115	127	BQDS	$5.53*10^{-4}$	$1.26*10^{-5}$
		ARS	$4.6*10^{-4}$	$1.05*10^{-5}$

Table S2 The key parameters and corresponding values of ranking for performance comparison between nanocellulose and Nafion 115 membranes.

Parameters for comparison	**Nanocellulose membrane**	**Nafion 115**
Low area-specific resistance	2 (3.29 Ω cm^2 in 1M H_2SO_4)	9 (0.73 Ω cm^2 in 1M H_2SO_4)
Tensile strength	9 (90 MPa)	3 (25 MPa)
Low electrolyte swelling ratio	4 (21.9 ± 1.7% in 1M H_2SO_4)	4 (19.6 ± 2.2% in 1M H_2SO_4)
Sustainability	8	2
Low permeability of redox species	8 (1.65×10^{-6} $cm^2\ h^{-1}$ for BQDS) (1.27×10^{-6} $cm^2\ h^{-1}$ for ARS)	1 (1.26×10^{-5} $cm^2\ h^{-1}$ for BQDS) (1.05×10^{-5} $cm^2\ h^{-1}$ for ARS)
Environmental friendliness	8	2

Note: Every parameter was quantitatively ranked from 1 to 10 to have a better comparison. The parameters except for sustainability and environmental friendliness were ranked according to the experimental results. For the Nafion membrane, the values for ranking in sustainability and environmental friendliness were very low because its production and by-products perfluoroalkyl and polyfluoroalkyl substances (PFASs) have a harmful influence on the environment and human health. Some EU countries have proposed or decided on the restriction on polyfluorinated chemicals. (https://echa.europa.eu/hot-topics/perfluoroalkyl-chemicals-pfas)